BMC Medical Imaging

RESEARCH Open Access

Preoperative prediction of lymph node metastasis in intrahepatic cholangiocarcinoma: an integrative approach combining ultrasound-based radiomics and inflammation-related markers

Yu-ting Peng[1†], Jin-shu Pang[1†], Peng Lin[2], Jia-min Chen[1], Rong Wen[1], Chang-wen Liu[1], Zhi-yuan Wen[1], Yu-quan Wu[1], Jin-bo Peng[1], Lu Zhang[3], Hong Yang[1], Dong-yue Wen[1*] and Yun He[1*]

Abstract

Objectives To develop ultrasound-based radiomics models and a clinical model associated with inflammatory markers for predicting intrahepatic cholangiocarcinoma (ICC) lymph node (LN) metastasis. Both are integrated for enhanced preoperative prediction.

Methods This study retrospectively enrolled 156 surgically diagnosed ICC patients. A region of interest (ROI) was manually identified on the ultrasound image of the tumor to extract radiomics features. In the training cohort, we performed a Wilcoxon test to screen for differentially expressed features, and then we used 12 machine learning algorithms to develop 107 models within the cross-validation framework and determine the optimal radiomics model through receiver operating characteristic (ROC) curve analysis. Multivariable logistic regression analysis was used to identify independent risk factors to construct a clinical model. The combined model was established by combining ultrasound-based radiomics and clinical parameters. The Delong test and decision curve analysis (DCA) were used to compare the diagnostic efficacy and clinical utility of different models.

Results A total of 1239 radiomics features were extracted from the ROIs of tumors. Among the 107 prediction models, the model (Stepglm + LASSO) utilizing 10 radiomics features ultimately yielded the highest average area under the receiver operating characteristic curve (AUC) of 0.872, with an AUC of 0.916 in the training cohort and 0.827 in the validation cohort. The combined model, which incorporates the optimal radiomics score, clinical N stage, and platelet-to-lymphocyte ratio (PLR), achieved an AUC of 0.882 in the validation cohort, significantly outperforming

†Yu-ting Peng and Jin-shu Pang contributed equally to this work and share first authorship.

*Correspondence:
Dong-yue Wen
844653793@qq.com
Yun He
heyun@stu.gxmu.edu.cn

Full list of author information is available at the end of the article

© The Author(s) 2024. **Open Access** This article is licensed under a Creative Commons Attribution-NonCommercial-NoDerivatives 4.0 International License, which permits any non-commercial use, sharing, distribution and reproduction in any medium or format, as long as you give appropriate credit to the original author(s) and the source, provide a link to the Creative Commons licence, and indicate if you modified the licensed material. You do not have permission under this licence to share adapted material derived from this article or parts of it. The images or other third party material in this article are included in the article's Creative Commons licence, unless indicated otherwise in a credit line to the material. If material is not included in the article's Creative Commons licence and your intended use is not permitted by statutory regulation or exceeds the permitted use, you will need to obtain permission directly from the copyright holder. To view a copy of this licence, visit http://creativecommons.org/licenses/by-nc-nd/4.0/.

the clinical model with an AUC of 0.687 ($P = 0.009$). According to the DCA analysis, the combined model also showed better clinical benefits.

Conclusions The combined model incorporating ultrasound-based radiomics features and the PLR marker offers an effective, noninvasive intelligence-assisted tool for preoperative LN metastasis prediction in ICC patients.

Clinical trial number Not applicable.

Keywords Intrahepatic cholangiocarcinoma, Lymph node metastasis, Radiomics, Ultrasound, Inflammation-related marker

Introduction

Intrahepatic cholangiocarcinoma (ICC) is one of the most aggressive tumors and is the second most common primary liver malignancy (approximately 15%), with an increasing incidence in recent years [1]. Surgical resection remains the sole curative treatment for ICC patients, yet the high likelihood of postoperative recurrence and metastasis leads to generally low 5-year overall survival rates [2, 3]. Notably, lymph node (LN) metastasis is a crucial factor that influences prognosis posthepatectomy for ICC, with a significant decrease in the 5-year survival rate to less than 20% for patients with positive LN status [4–6]. Research has demonstrated that for these LN-positive ICC patients, postoperative adjuvant chemoradiotherapy may confer survival benefits [2, 7]. Hence, accurate assessment of LN metastasis holds paramount importance for prognostic evaluation and guiding treatment selection in ICC patients.

Surgical pathology is the gold standard for diagnosing LN metastasis [8]. Imaging examinations play an important role as noninvasive tools. However, traditional imaging methods, such as ultrasound, CT, and MR, do not perform satisfactorily in diagnosing LN metastasis, and their sensitivity and specificity often fail to meet clinical satisfaction standards [9, 10]. Therefore, for ICC patients, accurately predicting LN metastasis prior to surgery is an important issue that is currently faced in clinical practice.

Radiomics, a pioneering image analysis technique, transforms medical images into quantitative features invisible to the naked eye, offering insights into the intricate pathophysiological states of tumors. This approach shows great potential in characterizing tumor phenotypes and improving cancer diagnosis, prognosis and treatment response [11, 12]. Recent studies have shown the capability of radiomics features in forecasting LN metastasis among biliary tract cancer patients, opening up novel research perspectives and possibilities in this domain [13]. Ultrasound examination is a prominent first-line examination method for assessing focal liver lesions, with several notable advantages. It is convenient and noninvasive, but it is often limited by the interference of gastrointestinal gas when assessing ICC LN metastasis. However, ultrasound radiomics technology provides the possibility to overcome this technical limitation. Due to its powerful data processing ability, it is expected to overcome the limitations of traditional ultrasound and achieve more accurate and comprehensive assessment [14]. More notably, ultrasound radiomics has proven effective in predicting LN metastasis in several types of cancers, including pancreatic, ovarian, and cervical cancers [15–18]. However, to the best of our knowledge, no studies have been reported on the prediction of ICC LN metastasis via ultrasound imaging, and ultrasound radiomics prediction models have not been established.

Furthermore, the main risk factors for ICC are hepatolithiasis, viral hepatitis, and clonorchis sinensis infestation, which often lead to chronic inflammation of the liver and bile ducts [19]. Chronic inflammation plays a pivotal role in the development and emergence of various cancers, including ICC [20, 21]. Inflammation-related markers such as the prognostic nutritional index (PNI), lymphocyte-to-monocyte ratio (LMR), systemic immune-inflammation index (SII), neutrophil-to-lymphocyte ratio (NLR), and platelet-to-lymphocyte ratio (PLR) can be used to assess the inflammatory and immune status of patients with tumors and have been widely employed in evaluating the prognosis of patients with ICC [22–24]. However, few studies have investigated the use of inflammation-related markers to predict ICC LN metastasis. Thus, exploring their potential in predicting ICC LN metastasis holds significant clinical importance.

Therefore, we sought to develop a predictive model that utilizes both ultrasound radiomics features and serum inflammatory markers, with the ultimate goal of precisely preoperatively identifying ICC LN metastasis.

Materials and methods

Research patients

This retrospective study was approved by the Ethics Committee of the First Affiliated Hospital of Guangxi Medical University. We reviewed a dataset spanning from January 2017 to June 2024 that included ICC patients who underwent hepatectomy at the First Affiliated Hospital of Guangxi Medical University. It adhered to the reporting guidelines outlined by the CheckList for EvaluAtion Radiomics research (CLEAR) and METhodological RadiomICs Score (METRICS) (Supplementary Material 1

and 2) [25, 26]. Patients were included based on the following criteria: (i) histologically confirmed ICC. and(ii) ultrasound examination was performed within 2 weeks before surgery. The exclusion criteria were as follows: (i) the target lesion was not fully and clearly displayed on the ultrasound image; (ii) previous cancer treatment history; (iii) incomplete baseline data; and (iv) absence of pathological information on the LNs. The detailed inclusion/exclusion criteria and recruitment process, as well as the sample size, are shown in Fig. 1a. Patients were randomly distributed into training cohort and validation cohort at a 7:3 ratio (Fig. 1b).

The following preoperative clinical parameters of ICC patients were collected and recorded: sex, age, tumor size, clinical N stage, hepatitis B virus (HBV) infection, clonorchis sinensis infection, hepatolithiasis, alpha fetoprotein (AFP), carcinoembryonic antigen (CEA), carbohydrate antigen 199 (CA199), NLR, PLR, SII, PNI, LMR, and LN metastasis. Clinical N stage was confirmed by abdominal ultrasound examination and enhanced abdominal magnetic resonance Imaging (MRI)/CT examination [27]. The absolute neutrophil count, absolute lymphocyte count, absolute platelet count, and absolute monocyte count were used to calculate inflammation-related markers in the peripheral blood. The formula for SII and PNI is as follows: SII = platelet count* NLR; PNI= (albumin + 5) * lymphocyte count.

Ultrasound examination

The ultrasound examinations were conducted using the following equipment: Resona 7 (Mindray, Shenzhen, China) and Logiq E9 (GE, Wauwatosa, USA). An abdominal probe was used to clearly visualize the lesions. Subsequently, the ultrasound image depicting the largest cross-section of the lesion was selected and saved in DICOM format.

Radiomics analysis

The radiomics research workflow encompasses steps like tumor lesion segmentation, feature extraction, feature selection and model development, and evaluation. (Fig. 2).

Lesion segmentation

For patients with multiple liver lesions, the largest lesion was evaluated. A 5-year experienced radiologist, proficient in abdominal ultrasound diagnosis, manually delineated the tumor's region of interest (ROI) via the polygon mode in ITK-SNAP software (version 4.2.0), and the delineation was subsequently verified by another radiologist with 12 years of ultrasound examination expertise. Upon encountering disagreements, the images were re-evaluated by a third expert radiologist with 15 years of experience in abdominal ultrasound diagnosis, to reach a final consensus. All radiologists were blinded to the pathological findings.

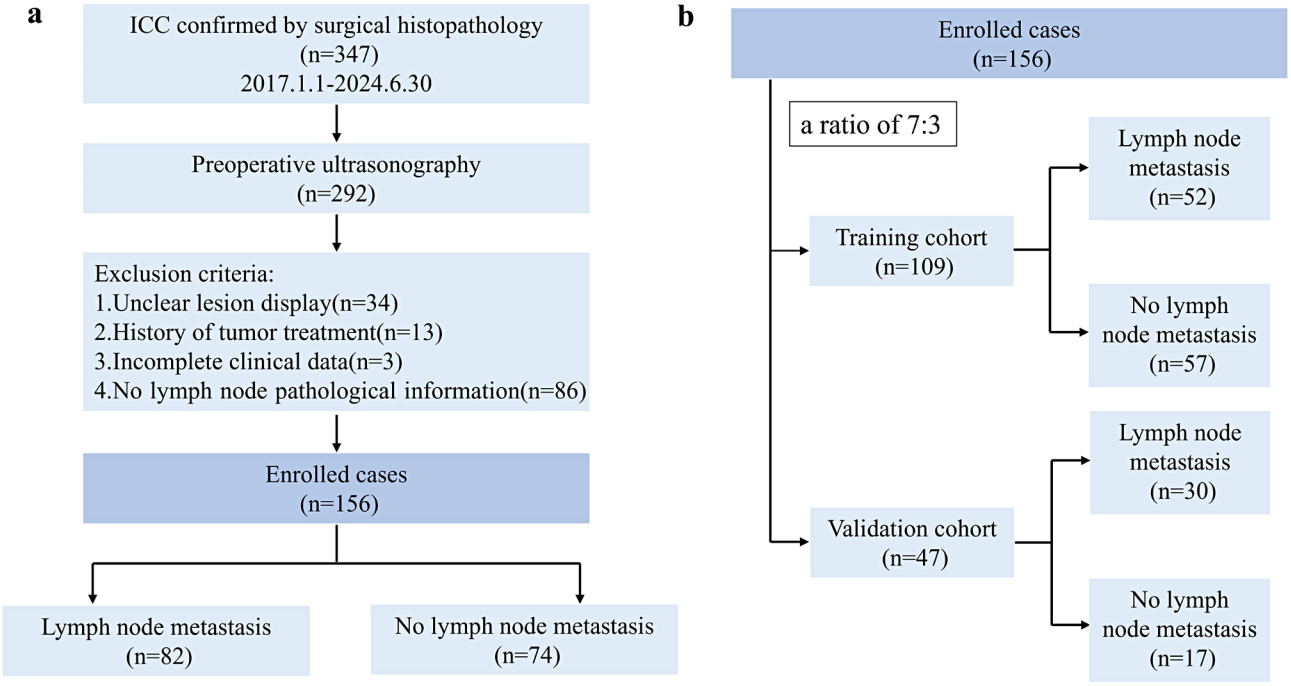

Fig. 1 Patient recruitment and grouping for the study. (**a**) According to the inclusion and exclusion criteria of the study, 82 patients with LN metastasis and 74 patients without LN metastasis were ultimately included. (**b**) Grouping of the patients

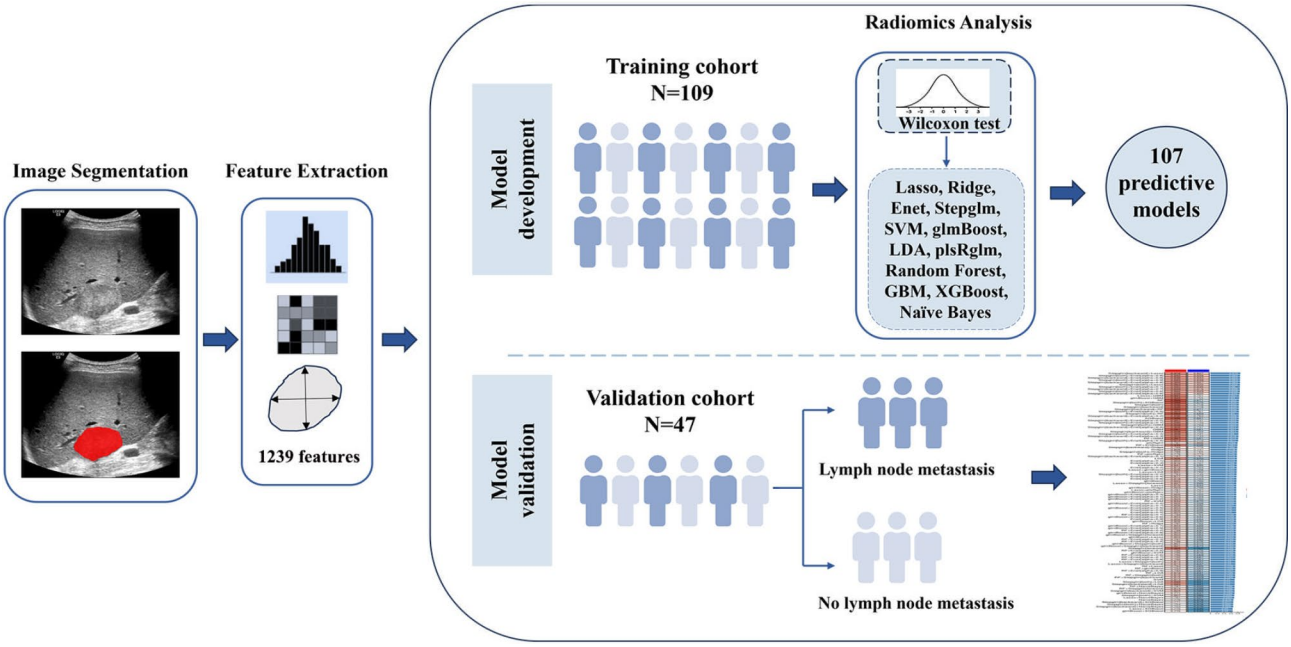

Fig. 2 Workflow of the radiomics analysis

Feature extraction

Radiomics features were extracted from the ROIs via the open-source software PyRadiomics (version 3.0.1), including shape features and first-order, second-order and higher-order features [28]. The second-order features encompassed the following five categories: (1) gray-level co-occurrence matrix (GLCM), which captures spatial relationships between gray levels; (2) gray-level run length matrix (GLRLM), which analyzes runs of pixels with the same gray level; (3) gray-level size zone matrix (GLSZM), which examines zones of similar gray levels and their sizes; (4) Neighboring gray tone difference matrix (NGTDM), which measures differences in gray tones between neighboring pixels; and (5) gray-level dependence matrix (GLDM) features, which were employed to assess the dependency of gray levels within an image. Higher-order features refer to image feature variables extracted by adding filters, including wavelets, logarithms, squares, square roots and exponentials. A bin width of 25 was utilized as a fixed value for discretizing the image's grey levels.

Feature selection and radiomics model development

After feature extraction, Z score normalization was performed to transform the features into a more uniform measure for comparison. The Z score was calculated via the following formula: Z=(x-mean(x))/std(x). Mean(x) represents the mean value of the radiomics feature in all samples, and std(x) represents the standard deviation of the feature in all samples. In the training cohort, we performed a Wilcoxon test to screen for differentially expressed features for subsequent analyses.

We subsequently used the following 12 machine learning algorithms to build radiomics models: plsRglm, least absolute shrinkage and selection operator (LASSO), ridge regression, gradient boosting machine (GBM), Stepglm, SVM, glmBoost, linear discriminant analysis (LDA), random forest, XGBoost, Enet, and naive Bayes. In the framework of cross-validation, one algorithm was used for variable selection, and another algorithm was used to construct classification prediction models.

This diverse array of algorithms allowed for an exhaustive exploration of modeling strategies, which resulted in the formulation of 107 integrated prediction radiomics models. Ultimately, the combination of machine learning techniques that demonstrated the highest average area under the receiver operating characteristic curve (AUC) emerged as the best model, which we designated the radiomics score. To reduce the risk of overfitting, we used 10-fold cross-validation to train the model.

In addition, to assess the reproducibility and generalization of radiomics features, tumor ROI was mapped from ultrasound images of 30 randomly selected patients by two physicians (5-year and 12-year experienced radiologists) to assess reproducibility between observers.

Development and evaluation of clinical and combined models

We developed models based on the training cohort. First, parameters with $P<0.1$ from univariable logistic regression analysis were selected for subsequent analysis. The

independent risk factors of ICC LN metastasis were determined by multivariable analysis ($P<0.05$), which were used to construct a clinical model. The combined model was subsequently constructed via logistic regression between the radiomics score and the parameters of the clinical model. To enhance clinical applicability, a nomogram was designed, presenting a straightforward and intuitive visualization of the predictive prowess in the combined model.

To evaluate the performance of the different models, their AUC values were calculated separately, and pairwise comparisons were performed via the Delong test. Moreover, decision curve analysis (DCA) was employed to assess the clinical utility of the model by demonstrating its ability to enhance decision-making processes.

Statistical analysis

MedCalc (version 18.2.1) and R statistical software (version 4.4.1) were used in our research.

To analyze and compare differences among categorical variables across different groups, a chi-square test of independence was employed. Continuous parameters were analyzed via t-tests or Mann–Whitney U tests. The maximum Youden index, representing the point nearest to the top left of the ROC curve, was utilized to ascertain the sensitivity, specificity, and other diagnostic performance indicators of various models, along with the optimal cutoff thresholds for inflammation-related biomarkers. For all tests, a P value less than 0.05 was considered statistically significant. The sample size was estimated using the PASS software (version 15), as detailed in Supplementary Material 3.

Results

Patient characteristics

A total of 156 ICC patients (88 males and 68 females), ranging in age from 26 to 68 years (mean 56.2±11.2 years), were recruited for our study. Among these patients, 52 with LN metastasis and 57 without LN metastasis were allocated to the training cohort ($n=109$), whereas 30 with LN metastasis and 17 without LN metastasis were assigned to the validation cohort ($n=47$). All of the ICC lesions included in the study were larger than 1 cm in diameter. The clinical parameters of the training and validation cohorts are summarized in Table 1. Among all the clinical parameters, HBV infection and the PNI were significantly different between groups ($P<0.05$).

Preoperative clinical N stage was not correctly determined in 41 patients (26.3%), of whom 24 patients without LN metastasis were judged as cN1 stage and 17 patients with LN metastasis were judged as cN0 stage.

Radiomics model construction

A total of 1239 radiomics features were extracted from each patient's ultrasound image. In the training cohort, a Spearman correlation analysis revealed that the radiomics features exhibited internal correlations and heterogeneity, as illustrated by the heatmap of radiomics features clustering (Fig. 3). Based on the radiomic features of patients in the training cohort, the Wilcoxon test identified 31 differentially expressed radiomics features for inclusion in subsequent machine learning analyses. We developed a total of 107 radiomics models by integrating 12 algorithms with either variable screening or model building techniques. The AUC values of each model were calculated and then ranked in descending order based on the average AUC (Fig. 4).

The top 10 models had AUC values of at least 0.80 for both the training and validation cohorts, and the diagnostic efficiency of these radiomics models was presented in Supplementary Material 3: Table S1. The best model was the combination of Stepglm (direction=backward) and LASSO, which had the highest average AUC (0.872), with AUCs of 0.916 (training) and 0.827 (validation), respectively.

We also counted the radiomics features used by the 107 models and summarized the frequency of these features to identify the important radiomics features for LN metastasis (Fig. 5a). The radiomics features and numbers included in the top 10 models are shown in Fig. 5b. Among them, the optimal model is constructed with 10 high-order features. The intra-class correlation coefficient of these 10 radiomic features was greater than 0.80, indicating satisfactory reproducibility between observers (Supplementary Material 3: Table S2).

Clinical and combined model construction

Univariable analysis revealed several risk factors, including clinical N stage; CA199, CEA, NLR, PLR, SII, PNI, and LMR, with p values less than 0.1. Multivariable analysis revealed that clinical N stage (OR=11.565, 95% CI 3.844–34.788) and PLR (OR=5.140, 95% CI 1.214–21.761) were independent clinical risk factors for LN metastasis in ICC patients (Table 2, both $P<0.05$), and these parameters were used to construct the clinical model.

The clinical model parameters (clinical N stage and PLR) were subsequently combined with the radiomics score via logistic regression to develop a combined model. Furthermore, the combined model was presented as a nomogram, providing a user-friendly and visually intuitive aid for clinical application (Fig. 6).

Assessment and comparison of model diagnostic efficacy

This study developed three approaches: a clinical one, a radiomics-based, and a combined approach. The

Table 1 Clinical parameters of the ICC patients

Parameters	Training cohort ($n=109$)	Validation cohort ($n=47$)	*P*-value
Sex			0.856
Male	62(56.88)	26(55.32)	
Female	47(43.12)	21(44.68)	
Age			0.526
≤ 60	73(66.97)	29(61.70)	
> 60	36(33.03)	18(38.30)	
Tumor size (cm)			0.662
≤ 5	31(28.44)	15(31.91)	
> 5	78(71.56)	32(68.09)	
Clinical N stage			0.140
N0	51(46.79)	16(34.04)	
N1	58(53.21)	31(65.96)	
HBV infection			0.042
Negative	65(59.63)	36(76.60)	
Positive	44(40.37)	11(23.40)	
Clonorchis sinensis infestation			0.413
Negative	79(72.48)	31(65.96)	
Positive	30(27.52)	16(34.04)	
Hepatolithiasis			0.389
Negative	98(89.91)	40(85.11)	
Positive	11(10.09)	7(14.89)	
AFP (ng/ml)			0.802
≤ 20	101(92.66)	43(91.49)	
> 20	8(7.34)	4(8.51)	
CA199 (U/ml)			0.133
≤ 37	56(51.38)	18(38.30)	
> 37	53(48.62)	29(61.70)	
CEA (ng/ml)			0.195
≤ 5	70(64.22)	25(53.19)	
> 5	39(35.78)	22(46.81)	
LN metastasis			0.064
No	57(52.29)	17(36.17)	
Yes	52(47.71)	30(63.83)	
NLR			0.067
≤ 2.35	42(38.53)	11(23.40)	
> 2.35	67(61.47)	36(76.60)	
PLR			0.528
≤ 214.59	84(77.06)	34(72.34)	
> 214.59	25(22.94)	13(27.66)	
SII			0.089
≤ 490.34	30(27.52)	7(14.89)	
> 490.34	79(72.48)	40(85.11)	
PNI			0.044
≤ 95.69	85(77.98)	43(91.49)	
> 95.69	24(22.02)	4(8.51)	
LMR			0.137
≤ 2.24	33(30.28)	20(42.55)	
> 2.24	76(69.72)	27(57.45)	

Values were shown as the number of patients (percentage). HBV, hepatitis B virus; AFP, alpha fetoprotein; CA199, carbohydrate antigen 199; CEA, carcinoembryonic antigen; LN, lymph node; NLR, neutrophil-to-lymphocyte ratio; PLR, platelet-to-lymphocyte ratio; SII, systemic immune-inflammation index; PNI, prognostic nutritional index; LMR, lymphocyte-to-monocyte ratio

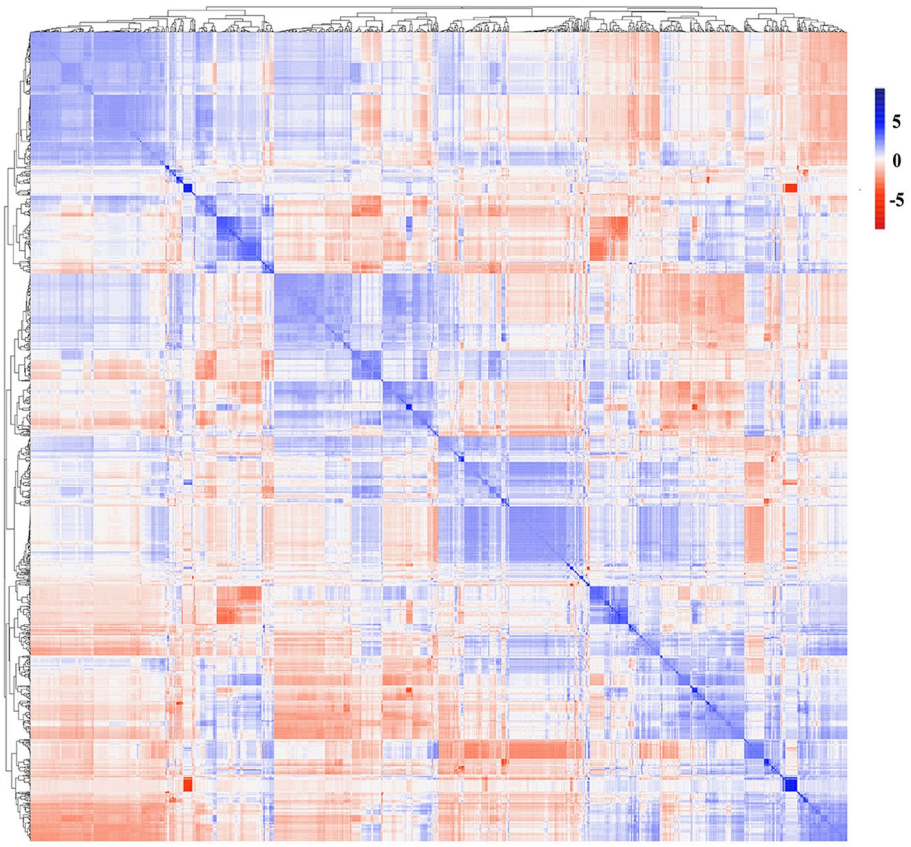

Fig. 3 Cluster heatmap of radiomics features based on ultrasound medicine images Z-score normalization was applied to scale the quantitative expression values of 1239 extracted radiomics characteristics, and heatmap visualization was utilized to demonstrate the clustering patterns among these radiomics characteristics

sensitivity and specificity were 78.8% (95%CI 0.653–0.889) and 70.2% (95%CI 0.566 0.816) for the clinical model, 94.2% (95%CI 0.841–0.988) and 73.7% (95%CI 0.603–0.845) for the radiomics model, and 98.1% (95%CI 0.897-1.000) and 86.0% (95%CI 0.742–0.937) for the combined model in the training cohort. In the validation cohort, the sensitivity and specificity were 80.0% (95%CI 0.614–0.923) and 58.8% (95%CI 0.329–0.816) for the clinical model, 80.0% (95%CI 0.614–0.923) and 76.5% (95%CI 0.501–0.932) for the radiomics model, and 83.3% (95%CI 0.653–0.944) and 82.4% (95%CI 0.566–0.962) for the combined model (Table 3).

In evaluating the predictive power of our models, the AUC values of different models in the training and validation cohort showed differences (Fig. 7a-b). The DeLong test revealed that the AUC value of the combined model was greater than that of the clinical model in both the training cohort (0.969 vs. 0.803, $P<0.001$) and the validation cohort (0.882 vs. 0.687, $P=0.009$) (Table 4). In the training cohort, the AUC of the combined model was greater than that of the radiomics model (0.969 vs. 0.916, $P=0.015$), and the AUC of the radiomics model was greater than that of the clinical model (0.916 vs. 0.803, $P=0.022$). In the validation cohort, none of the differences were statistically significant (radiomics vs. combined, clinical vs. radiomics, both $P>0.05$). Compared with the clinical model, the DCA demonstrated that both the radiomics model and the combined model had superior clinical utility in the preoperative prediction of ICC LN metastasis (Fig. 7c-d). The confusion matrix of different models is shown in Fig. 8.

Discussion

Accurate preoperative diagnosis of LN metastasis is crucial in refining the precise staging, prognostic evaluation, and guiding adjuvant therapy strategies for ICC patients [29]. This study introduced a novel model integrating ultrasound radiomics with serological inflammation-related markers, demonstrating moderate diagnostic effectiveness. This suggests its potential as a noninvasive preoperative tool for predicting LN metastasis in ICC.

The PLR, defined as the quotient of the absolute platelet count divided by the absolute lymphocyte count, is a crucial serological inflammatory marker. The nonspecific inflammatory response induced by malignancy often manifests as an elevation in platelet levels and a decrease

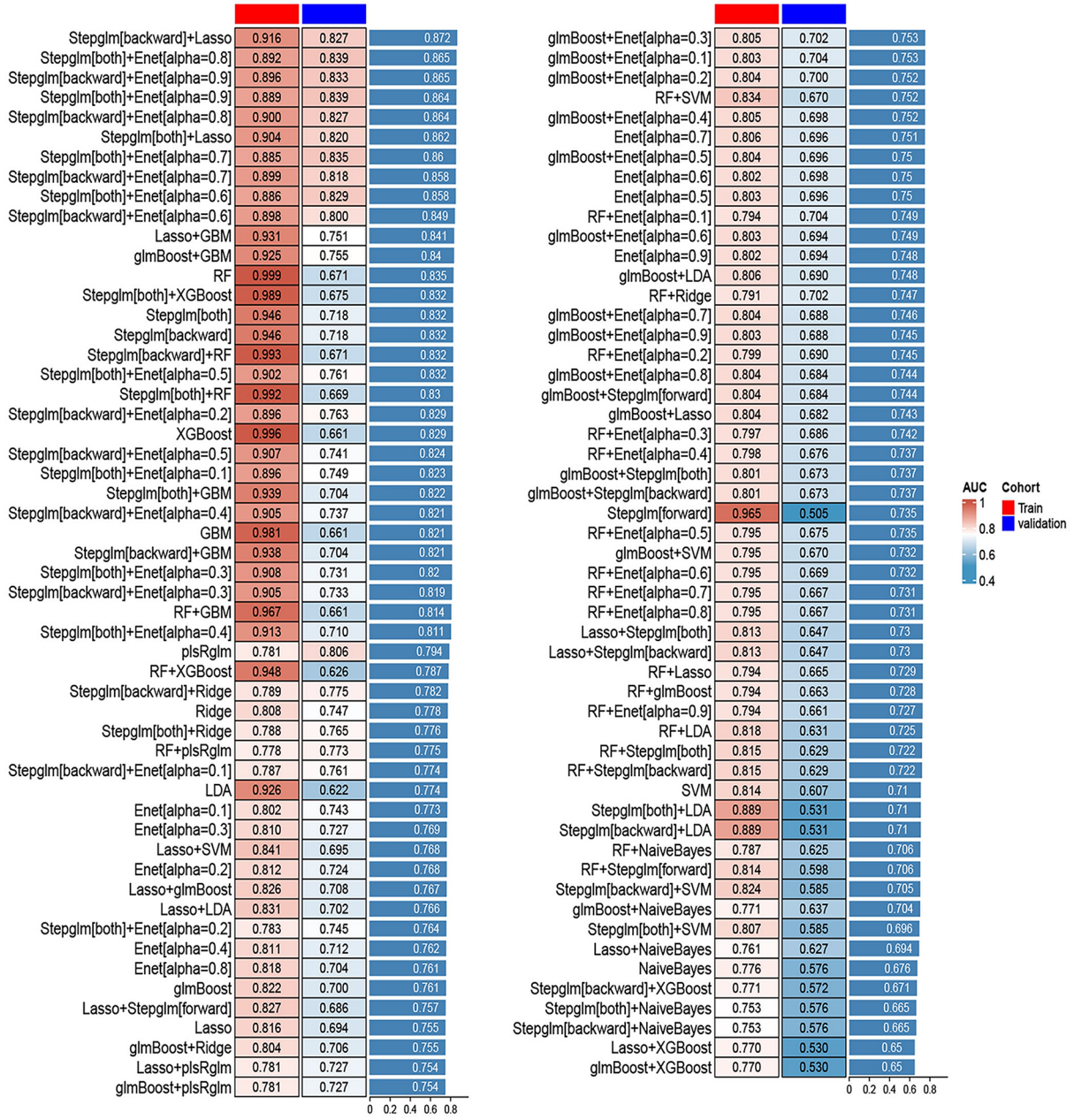

Fig. 4 Predictive models were developed and validated by screening radiomics features with machine learning algorithms. A total of 107 predictive models were constructed, and the AUC values of each model in the training and validation cohorts and their average AUC values were calculated and ranked in descending order of average AUC values. The performance of each model is presented through three key indicators: Training cohort AUC, Validation cohort AUC, and their average. Average AUC= (training cohort AUC + validation cohort AUC) /2

in lymphocytes. Platelets promote tumor progression by secreting tumor necrosis factor (TNF), vascular endothelial growth factor (VEGF) and platelet-derived factors [30]. Lymphocytes inhibit tumor growth, proliferation, and metastasis by mediating cytotoxic responses and releasing cytokines [31]. Previous studies have demonstrated that preoperative serological inflammatory markers are valuable for evaluating ICC patient prognosis as they indicate the balance between tumor-induced inflammation and the immune system's anti-tumor response [32, 33]. Moreover, Yu et al. developed nomograms based on the inflammation-related markers NLR and SII, which exhibited certain value in predicting ICC LN metastasis (C-index: 0.737 for internal validation and 0.674 for external validation) [34]. Our study created a clinical model based on the PLR and the clinical N stage, achieving AUC values of 0.803 and 0.687 in the training and validation cohorts, respectively. This diagnostic

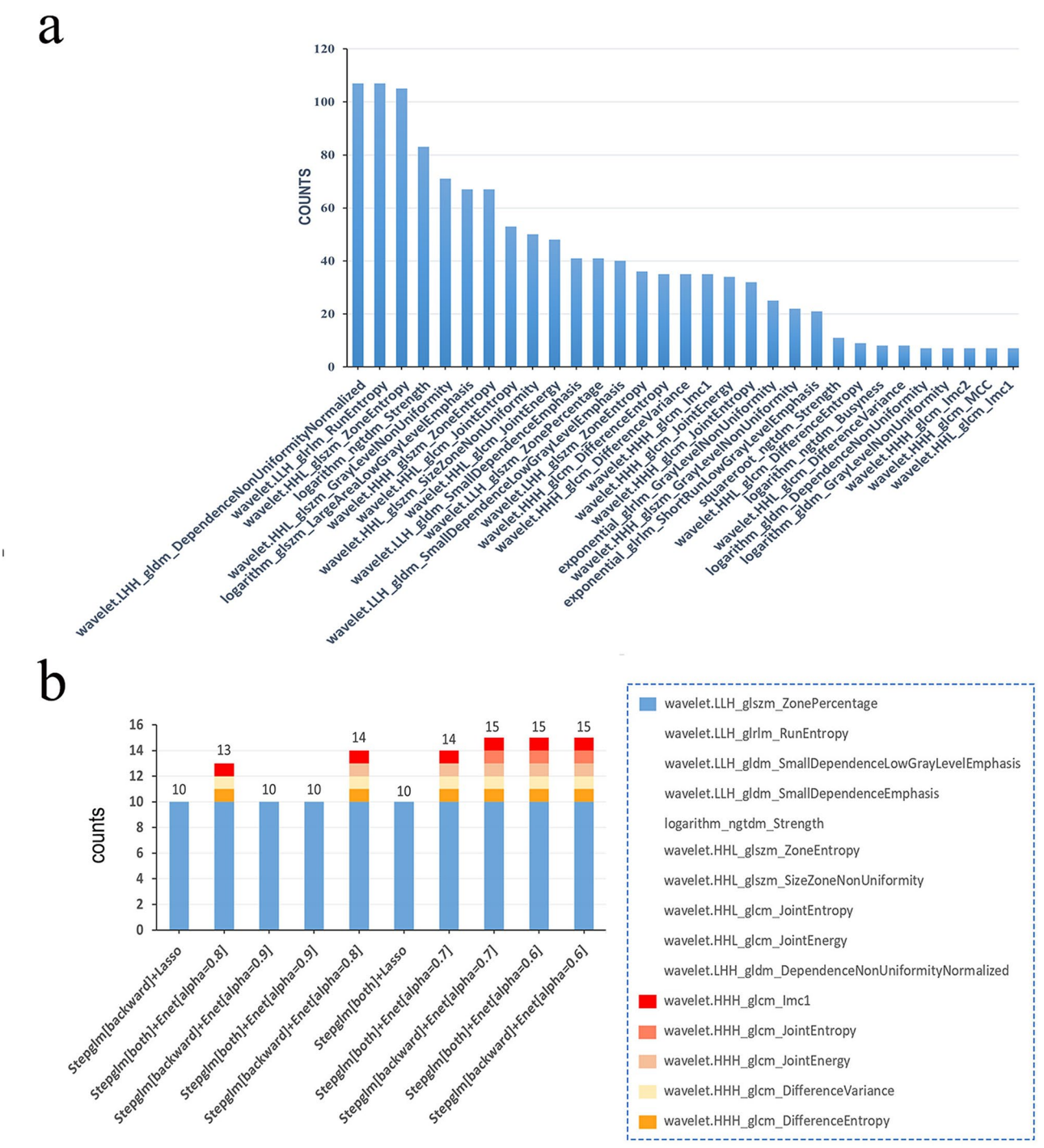

Fig. 5 The use of radiomics features in predictive models. (**a**) Statistics of the number of times radiomics features used in the 107 predictive models, identifying the important features for this study. (**b**) Radiomics features of the top 10 models. The vertical coordinate values represent the total number of features used to construct the model, the horizontal coordinates represent the model's name, and the bar graph colors represent the features used to construct the model

Table 2 Results of logistic regression analysis of ICC LN metastasis

Parameters	Univariable analysis OR (95%CI)	*P*-value	Multivariable analysis OR (95%CI)	*P*-value
Sex				
Male	Reference			
Female	0.694(0.324–1.490)	0.349		
Age				
≤ 60	Reference			
> 60	0.822(0.369–1.833)	0.632		
Tumor size (cm)				
≤ 5	Reference			
> 5	2.015(0.853–4.759)	0.110		
Clinical N stage				
N0	Reference		Reference	
N1	8.770(3.657–21.030)	<0.001	11.565(3.844–34.788)	<0.001
HBV infection				
Negative	Reference			
Positive	0.540(0.248–1.176)	0.120		
Clonorchis sinensis infestation				
Negative	Reference			
Positive	0.944(0.407–2.192)	0.893		
Hepatolithiasis				
Negative	Reference			
Positive	2.061(0.567–7.496)	0.272		
AFP (ng/ml)				
≤ 20	Reference			
> 20	1.104(0.262–4.660)	0.893		
CA199(U/ml)				
≤ 37	Reference		Reference	
> 37	2.016(0.940–4.325)	0.072	1.446(0.525–3.989)	0.476
CEA (ng/ml)				
≤ 5	Reference		Reference	
> 5	2.844(1.262–6.407)	0.012	2.519(0.886–7.163)	0.083
NLR				
≤ 2.35	Reference		Reference	
> 2.35	4.444(1.908–10.349)	0.001	0.960(0.224–4.112)	0.960
PLR				
≤ 214.59	Reference		Reference	
> 214.59	3.782(1.425–10.033)	0.008	5.140(1.214–21.761)	0.026
SII				
≤ 490.34	Reference		Reference	
> 490.34	5.576(2.051–15.158)	0.001	2.732(0.607–12.304)	0.191
PNI				
≤ 95.69	Reference		Reference	
> 95.69	0.213(0.073–0.623)	0.005	0.301(0.074–1.217)	0.092
LMR				
≤ 2.24	Reference		Reference	
> 2.24	0.326(0.138–0.769)	0.010	1.272(0.362–4.470)	0.708

OR: odds ratio; 95% CI: 95% confidence intervals; HBV, hepatitis B virus; AFP, alpha fetoprotein; CA199, carbohydrate antigen 199; CEA, carcinoembryonic antigen; NLR, neutrophil-to-lymphocyte ratio; PLR, platelet-to-lymphocyte ratio; SII, systemic immune-inflammation index; PNI, prognostic nutritional index; LMR, lymphocyte-to-monocyte ratio

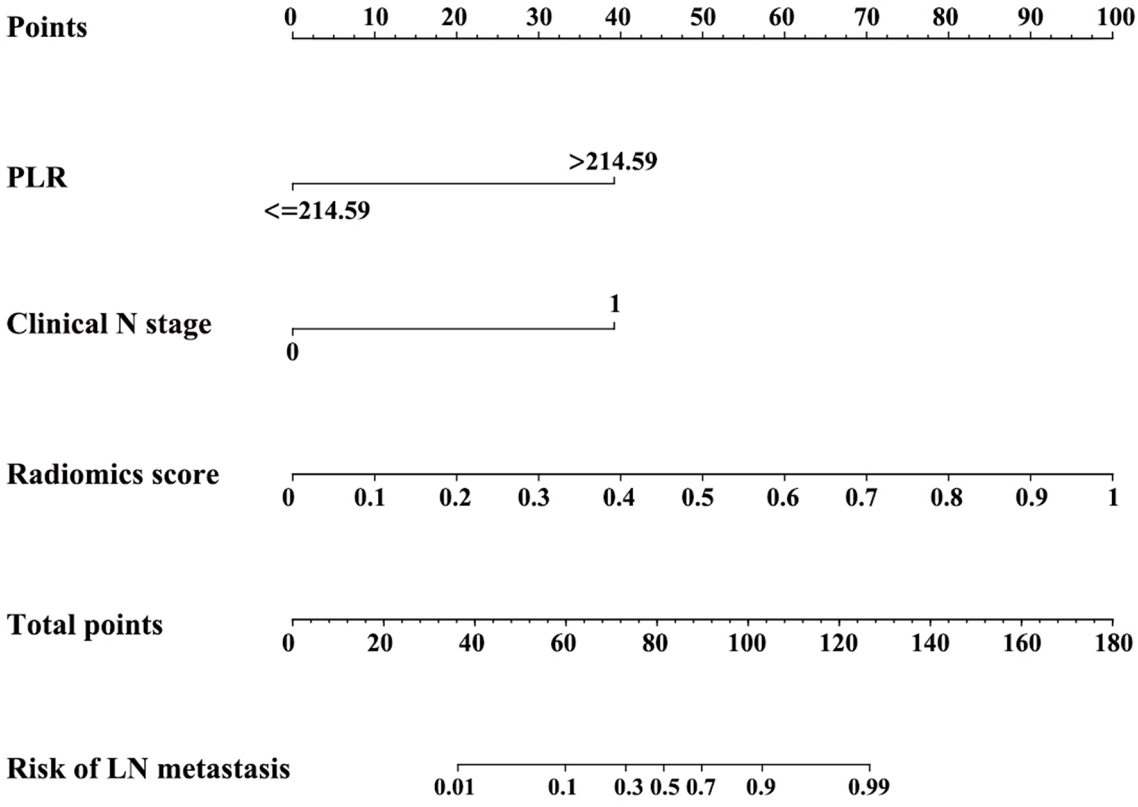

Fig. 6 Nomogram of the combined model for predicting LN metastasis in ICC

Table 3 Performance of different models for predicting LN metastasis in the training and validation cohorts

Cohort	Model	AUC (95% CI)	SEN (%)	SPE (%)	PPV (%)	NPV (%)	ACC (%)
Training	Clinical model	0.803 (0.721–0.886)	78.8	70.2	70.7	78.4	74.3
	Radiomics model	0.916 (0.865–0.966)	94.2	73.7	76.6	93.3	83.5
	Combined model	0.969 (0.943–0.995)	98.1	86.0	86.4	98.0	91.7
Validation	Clinical model	0.687 (0.523–0.851)	80.0	58.8	77.4	62.5	72.3
	Radiomics model	0.827 (0.709–0.946)	80.0	76.5	85.7	68.4	78.7
	Combined model	0.882 (0.786–0.979)	83.3	82.4	89.3	73.7	83.0

AUC, area under curve; 95% CI, 95% confidence intervals; SEN, sensitivity; SPE, specificity; PPV, positive predictive value; NPV negative predictive value; ACC, accuracy

performance is comparable to the results reported by Yu et al., suggesting that PLR has the potential to predict LN metastasis in ICC patients preoperatively.

Radiomics has been shown to be helpful for the noninvasive and individualized prediction of LN metastasis in ICC patients. Primary radiomics-related research on ICC LN metastasis currently focuses on utilizing CT and MR imaging, typically employing 1–3 machine learning techniques, and has shown promising initial outcomes. Ji et al. developed an LASSO-based radiomics model using enhanced CT images of 103 ICC patients, effectively predicting LN metastasis with AUC values of 0.823 (training) and 0.871 (validation) [35]. Qian et al. developed a model for predicting ICC LN metastasis using T2WI and delayed-phase T1WI images from 197 patients, incorporating mRMR and LASSO for radiomics feature selection. The model exhibited moderate performance, with an AUC of 0.701 [36]. Using a limited number of algorithms often poses challenges in comprehensively capturing the complex information within imaging data. Different from previous studies, our research incorporated a wider variety of machine learning algorithms (12 algorithms) and constructed multiple radiomics models (107 models) for comparison and selection to identify the optimal radiomics model. This strategy not only bolsters the model's adaptability to complex image information but also allows for deeper analysis and more extensive utilization of image data.

Ultrasound imaging boasts accessibility, simplicity, economy, and noninvasiveness, making it a frequently used first-choice medical imaging technique for examining liver conditions. Prior investigations have illustrated

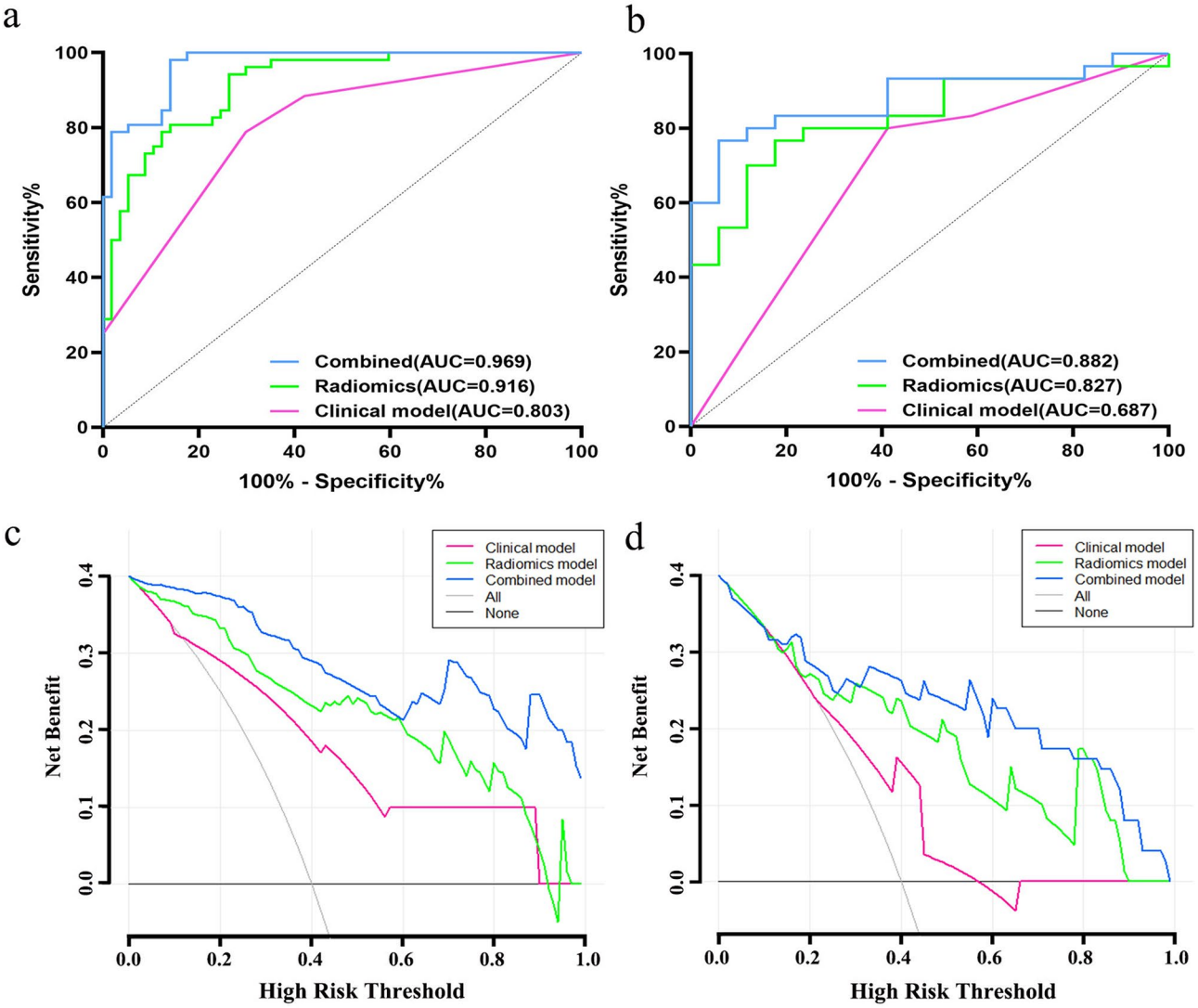

Fig. 7 Evaluation of the diagnostic performance of different models ROC curves for predicting LN metastasis were compared among the clinical, radiomics, and combined models in the training (**a**) and validation (**b**) cohorts. The DCA results for the three models are shown for the training (**c**) and validation (**d**) cohorts

Table 4 DeLong testing between different models

Model	Training cohort		Validation cohort	
	AUC (95% CI)	*P*-value	AUC (95% CI)	*P*-value
Clinical model	0.803 (0.721–0.886)		0.687 (0.523–0.851)	
Radiomics model	0.916 (0.865–0.966)		0.827 (0.709–0.946)	
Combined model	0.969 (0.943–0.995)		0.882 (0.786–0.979)	
Clinical model VS Radiomics model		0.022		0.197
Radiomics model VS Combined model		0.015		0.219
Clinical model VS Combined model		<0.001		0.009

AUC, area under curve; 95% CI, 95% confidence intervals

the utility of ultrasound-based radiomics in predicting pathological characteristics [37, 38]. However, research that explores the potential of ultrasound radiomics in predicting ICC LN metastasis is currently insufficient. In our research, through numerous attempts and comparisons of various algorithms, we explored suitable algorithm combinations for ultrasound image analysis. Ultimately, we found that the combination of Stepglm (direction=backward) and LASSO performed optimally, with the highest average AUC values (0.872) in

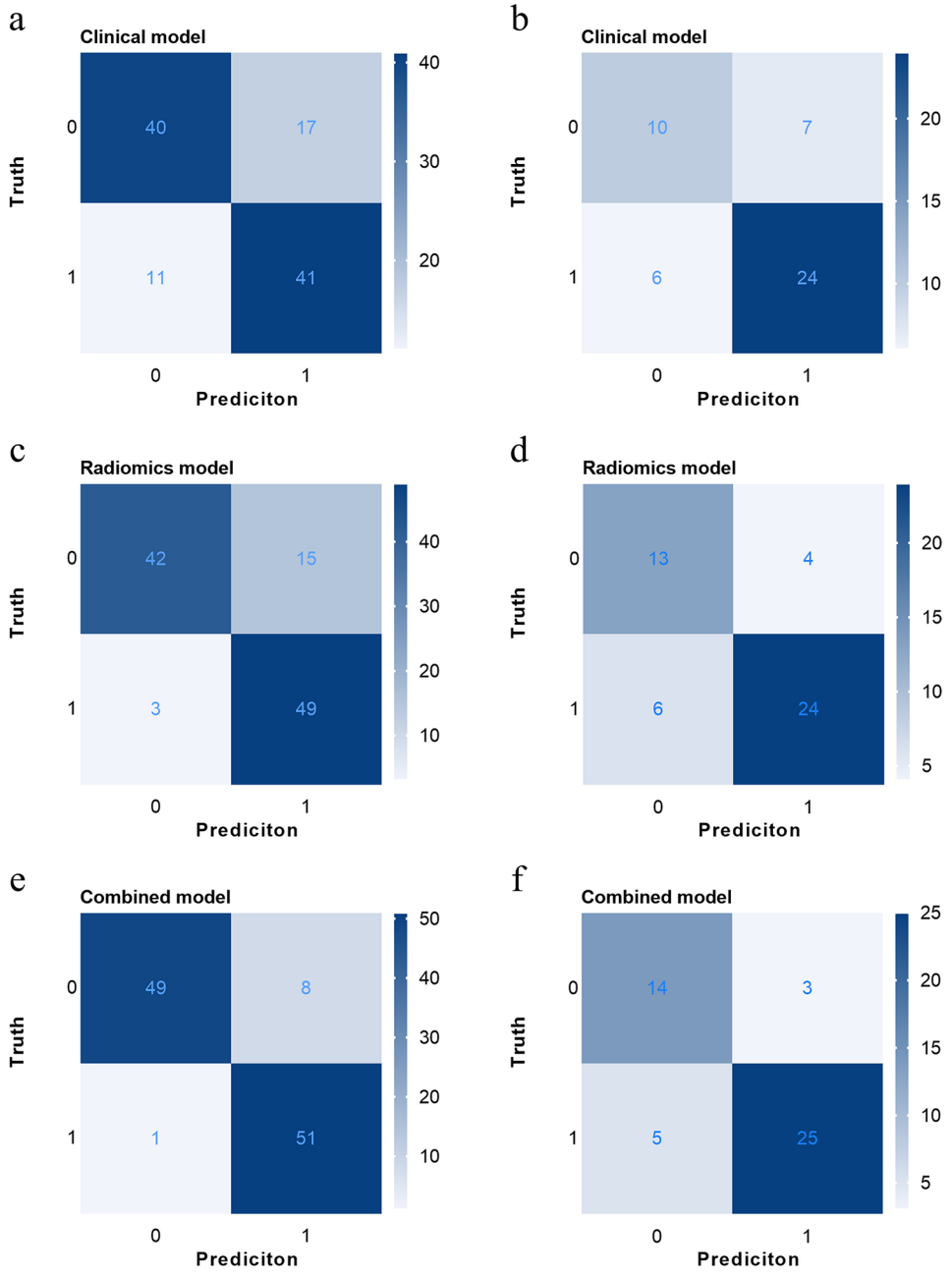

Fig. 8 Confusion matrices for different models. Clinical model training cohort (**a**) and validation cohort (**b**). Radiomics model training cohort (**c**) and validation cohort (**d**). Combined model training cohort (**e**) and validation cohort (**f**). The horizontal coordinate represents the predicted label, and the vertical coordinate represents the real label. label 0: no lymph node metastasis, label 1: lymph node metastasis

the training cohort (0.916) and validation cohort (0.872). This discovery indicates that ultrasound radiomics has significant potential and value in predicting LN metastasis in ICC. The optimal model consisted of 10 high-order radiomic features, nine of which were obtained through wavelet transformation, while one feature was derived from logarithm transformation. Wavelet transformation, which can reveal intricate layers of detail and information content within images, is widely employed in radiomics research [39–41]. Logarithm transformation enhances contrast by expanding lower grey levels and compressing higher ones, enabling clearer detail visualization in darker image regions [42]. The features "wavelet.LHH_gldm_DependenceNonUniformityNormalized" and "wavelet.LLH_glrlm_RunEntropy" were the most frequently utilized in our modeling process. In Granata et al.'s study, the DependenceNonUniformityNormalized feature, categorized under gldm, was found to be helpful

in distinguishing between the expansive and infiltrative fronts of tumour growth [43]. The RunEntropy quantifies uncertainty in run lengths and gray levels, indicating pixel arrangement unpredictability and offering insights into image texture and complexity [44]. However, the clinical or biological significance of these features still needs to be further studied and validated.

The combined model incorporating ultrasound radiomics features and serum inflammation-related indicators in our study possesses wider applicability and clinical value than a standalone model intended for preoperative, non-invasive evaluation of LN metastasis. However, upon applying the DeLong test for analysis, a noteworthy observation emerged. The AUC values did not significantly differ between the radiomics model and the clinical model in the validation cohort. Similarly, the comparison between the combined and radiomics models yielded comparable results. We speculate that this finding could stem from the somewhat limited sample size within the validation cohort, underscoring the need for future studies to expand the sample size to validate this finding.

This work has several limitations. First, manually segmenting the ROI of the tumor is very time consuming, and automatic segmentation methods need to be applied in the future. Second, the prevalent presentation of ICC patients at advanced stages of the disease often restricts the pool of candidates eligible for surgical intervention, resulting in a comparatively modest number of ICC patients being recruited for our research. Additionally, being a single-center study further restricts the generalizability of our findings. Third, selection bias is inevitable in retrospective studies. Moreover, despite our efforts to ensure the accuracy of lymph node metastasis diagnosis by including only pathologically confirmed ICC cases, this approach introduced a potential verification bias. Prospective, multi-institutional studies that incorporate a more substantial patient cohort should be conducted in the future, thereby enabling a more rigorous validation of the robustness and reproducibility of our models. Fourth, reliance on traditional 2D ultrasound images for radiomics feature extraction may overlook crucial spatial and volumetric tumor information. Incorporating 3D ultrasound in future research is necessary to obtain more comprehensive imaging. Fifth, although this study selected representative inflammatory biomarkers to assess their roles in ICC LN metastasis, it did not encompass all possible indicators, resulting in an incomplete assessment. Future research will explore more biomarkers to enhance the precision of diagnostic and therapeutic recommendations.

Conclusion

In conclusion, we developed a combined model of ultrasound-based radiomics combined with the inflammation-related marker PLR. It is expected to be an effective tool for the preoperative nonintrusive evaluation of LN metastasis in ICC patients, contributing to precision medicine and personalized medicine.

Abbreviations

ICC	Intrahepatic cholangiocarcinoma
LN	Lymph node
ROI	Region of interest
ROC	Receiver operating characteristic
DCA	Decision curve analysis
PNI	Prognostic nutritional index
LMR	Lymphocyte-to-monocyte ratio
SII	Systemic immune-inflammation index
NLR	Neutrophil-to-lymphocyte ratio
PLR	Platelet-to-lymphocyte ratio
GLCM	Gray level co-occurrence matrix
GLRLM	Gray level run length matrix
GLSZM	Gray level size zone matrix
NGTDM	Neighbouring gray tone difference matrix
GLDM	Gray level dependence matrix
LASSO	Least absolute shrinkage and selection operator
GBM	Gradient Boosting Machine
GLDM	Gray level dependence matrix
LDA	Linear Discriminant Analysis
DCA	Decision curve analysis

Supplementary Information

The online version contains supplementary material available at https://doi.org/10.1186/s12880-024-01542-8.

Supplementary Material 1

Supplementary Material 2

Supplementary Material 3

Acknowledgements

We thank the Laboratory of Guangxi Zhuang Autonomous Region Engineering Research Center for Artificial Intelligence Analysis of Multimodal Tumor Images, Key Laboratory of Ultrasonic Molecular Imaging and Artificial Intelligence, Guangxi Key Laboratory of Early Prevention and Treatment for Regional High Frequency Tumor/Key Laboratory of Early Prevention and Treatment for Regional High Frequency Tumor (Guangxi Medical University), Ministry of Education for their support of this study.

Author contributions

PYT and PJS formulated the overarching research design as well as drafting the manuscript; LP, CJM, WR, LCW, WZY, WYQ, PJB, ZL and YH contributed to the acquisition, analysis and interpretation of data; WDY and HY made a critical commentary or revision of the paper. All authors read and approved the final manuscript.

Funding

This study was funded by the National Natural Science Foundation of China (No. 82160336).

Data availability

The dataset and analysis for this study can be obtained from the corresponding author upon reasonable request.

Declarations

Ethics approval and consent to participate
This retrospective study was conducted with approval from the Medical Ethics Committee of First Affiliated Hospital of Guangxi Medical University (No.2024-E421-01). The requirement of informed consent was waived by the Ethics Committee of First Affiliated Hospital of Guangxi Medical University owing to the retrospective nature of the study.

Consent for publication
Not applicable.

Study subjects or cohorts overlap
27 study subjects have been previously reported in:
Peng YT, Zhou CY, Lin P, et al. Preoperative Ultrasound Radiomics Signatures for Noninvasive Evaluation of Biological Characteristics of Intrahepatic Cholangiocarcinoma. Acad Radiol. 2020;27(6):785–797.

Competing interests
The authors declare no competing interests.

Author details
[1]Department of Medical Ultrasound, The First Affiliated Hospital of Guangxi Medical University, No.6 Shuangyong, Road, Nanning, Guangxi Zhuang Autonomous Region, China
[2]Department of Medical Ultrasound, Fujian Medical University Union Hospital, No.29 Xinquan road, Fuzhou, Fujian Province, China
[3]Department of Medical Pathology, The First Affiliated Hospital of Guangxi Medical University, No.6 Shuangyong, Road, Nanning, Guangxi Zhuang Autonomous Region, China

Received: 5 October 2024 / Accepted: 19 December 2024
Published online: 02 January 2025

References

1. Valle JW, Kelley RK, Nervi B, Oh DY, Zhu AX. Biliary tract cancer. Lancet. 2021;397(10272):428–44.
2. Mazzaferro V, Gorgen A, Roayaie S, Droz Dit Busset M, Sapisochin G. Liver resection and transplantation for intrahepatic cholangiocarcinoma. J Hepatol. 2020;72(2):364–77.
3. Chun YS, Javle M. Systemic and adjuvant therapies for Intrahepatic Cholangiocarcinoma. Cancer Control. 2017;24(3):1073274817729241.
4. Navarro JG, Lee JH, Kang I, et al. Prognostic significance of and risk prediction model for lymph node metastasis in resectable intrahepatic cholangiocarcinoma: do all require lymph node dissection? HPB (Oxford). 2020;22(10):1411–9.
5. Bridgewater J, Galle PR, Khan SA, et al. Guidelines for the diagnosis and management of intrahepatic cholangiocarcinoma. J Hepatol. 2014;60(6):1268–89.
6. European Association for the Study of the Liver. Electronic address eee, European Association for the study of the L. EASL-ILCA Clinical Practice guidelines on the management of intrahepatic cholangiocarcinoma. J Hepatol. 2023;79(1):181–208.
7. Horgan AM, Amir E, Walter T, Knox JJ. Adjuvant therapy in the treatment of biliary tract cancer: a systematic review and meta-analysis. J Clin Oncol. 2012;30(16):1934–40.
8. Lee AJ, Chun YS. Intrahepatic cholangiocarcinoma: the AJCC/UICC 8th edition updates. Chin Clin Oncol. 2018;7(5):52.
9. Krenzien F, Nevermann N, Krombholz A et al. Treatment of intrahepatic cholangiocarcinoma-A multidisciplinary approach. Cancers (Basel). 2022;14(2).
10. Ke Q, Wang L, Lin Z, et al. Prognostic value of Lymph Node Dissection for Intrahepatic Cholangiocarcinoma patients with clinically negative Lymph Node Metastasis: a Multi-center Study from China. Front Oncol. 2021;11:585808.
11. Gillies RJ, Kinahan PE, Hricak H. Radiomics: images are more than pictures, they are data. Radiology. 2016;278(2):563–77.
12. Lambin P, Leijenaar RTH, Deist TM, et al. Radiomics: the bridge between medical imaging and personalized medicine. Nat Rev Clin Oncol. 2017;14(12):749–62.
13. Laghi A, Voena C. CT-based Radiomics for biliary Tract Cancer: a possible solution for Predicting Lymph Node metastases. Radiology. 2019;290(1):99–100.
14. Brunese MC, Fantozzi MR, Fusco R et al. Update on the applications of Radiomics in diagnosis, staging, and recurrence of Intrahepatic Cholangiocarcinoma. Diagnostics (Basel). 2023;13(8).
15. Tang Y, Su YX, Zheng JM, et al. Radiogenomic analysis for predicting lymph node metastasis and molecular annotation of radiomic features in pancreatic cancer. J Transl Med. 2024;22(1):690.
16. Wen DY, Chen JM, Tang ZP, et al. Noninvasive prediction of lymph node metastasis in pancreatic cancer using an ultrasound-based clinicoradiomics machine learning model. Biomed Eng Online. 2024;23(1):56.
17. Qi Y, Liu J, Wang X, et al. Development and validation of an ultrasound–based radiomics nomogram to predict lymph node status in patients with high-grade serous ovarian cancer: a retrospective analysis. J Ovarian Res. 2024;17(1):48.
18. Jin X, Ai Y, Zhang J, et al. Noninvasive prediction of lymph node status for patients with early-stage cervical cancer based on radiomics features from ultrasound images. Eur Radiol. 2020;30(7):4117–24.
19. Banales JM, Marin JJG, Lamarca A, et al. Cholangiocarcinoma 2020: the next horizon in mechanisms and management. Nat Rev Gastroenterol Hepatol. 2020;17(9):557–88.
20. Mantovani A, Cancer. Inflaming Metastasis Nat. 2009;457(7225):36–7.
21. Massarweh NN, El-Serag HB. Epidemiology of Hepatocellular Carcinoma and Intrahepatic Cholangiocarcinoma. Cancer Control. 2017;24(3):1073274817729245.
22. Tsilimigras DI, Moris D, Mehta R, et al. The systemic immune-inflammation index predicts prognosis in intrahepatic cholangiocarcinoma: an international multi-institutional analysis. HPB (Oxford). 2020;22(12):1667–74.
23. Lv M, Wang K, Zhang Z, Zhang Z, Wan J. The predictive value of lymphocyte to monocyte ratio for overall survival in cholangiocarcinoma patients with hepatic resection. Cancer Med. 2023;12(8):9482–95.
24. Zhu J, Wang D, Liu C, et al. Development and validation of a new prognostic immune-inflammatory-nutritional score for predicting outcomes after curative resection for intrahepatic cholangiocarcinoma: a multicenter study. Front Immunol. 2023;14:1165510.
25. Kocak B, Baessler B, Bakas S, et al. CheckList for EvaluAtion of Radiomics research (CLEAR): a step-by-step reporting guideline for authors and reviewers endorsed by ESR and EuSoMII. Insights Imaging. 2023;14(1):75.
26. Kocak B, Akinci D'Antonoli T, Mercaldo N, et al. METhodological RadiomICs score (METRICS): a quality scoring tool for radiomics research endorsed by EuSoMII. Insights Imaging. 2024;15(1):8.
27. National Cancer C, Liver Cancer Expert Committee of National Cancer Quality Control C. [Quality control index for standardized diagnosis and treatment of primary liver cancer in China (2022 edition)]. Zhonghua Zhong Liu Za Zhi. 2022;44(7):600–8.
28. van Griethuysen JJM, Fedorov A, Parmar C, et al. Computational Radiomics System to Decode the Radiographic phenotype. Cancer Res. 2017;77(21):e104–7.
29. Ishii T, Iwaki K, Nakakura A, Yoh T, Uchida Y, Hatano E. Is routine lymph node dissection recommended for liver resection of intrahepatic cholangiocarcinoma? A systematic review and meta-analysis. HPB (Oxford). 2024;26(6):731–40.
30. Schlesinger M. Role of platelets and platelet receptors in cancer metastasis. J Hematol Oncol. 2018;11(1):125.
31. Ray-Coquard I, Cropet C, Van Glabbeke M, et al. Lymphopenia as a prognostic factor for overall survival in advanced carcinomas, sarcomas, and lymphomas. Cancer Res. 2009;69(13):5383–91.
32. Zhang Z, Zhou Y, Hu K, Huang Y. Investigating effects of preoperative inflammatory biomarkers on predicting survival outcomes of intrahepatic cholangiocarcinoma after curative resection. World J Surg Oncol. 2020;18(1):272.
33. Li H, Wang JJ, Zhang M, et al. Prognostic significance of systemic immune-inflammation index in patients with intrahepatic cholangiocarcinoma undergoing hepatic resection. World J Gastrointest Oncol. 2020;12(4):467–82.
34. Yu XP, Chen JL, Tang Y, et al. [A nomogram for preoperative prediction of lymph node metastasis in patients with intrahepatic cholangiocarcinoma based on inflammation-related markers]. Zhonghua Wai Ke Za Zhi. 2023;61(4):321–9.
35. Ji GW, Zhu FP, Zhang YD, et al. A radiomics approach to predict lymph node metastasis and clinical outcome of intrahepatic cholangiocarcinoma. Eur Radiol. 2019;29(7):3725–35.
36. Qian X, Ni X, Miao G et al. Association between MRI-Based Radiomics features and Regional Lymph Node Metastasis in Intrahepatic Cholangiocarcinoma and its clinical outcome. J Magn Reson Imaging. 2024.

37. Hu HT, Wang Z, Huang XW, et al. Ultrasound-based radiomics score: a potential biomarker for the prediction of microvascular invasion in hepatocellular carcinoma. Eur Radiol. 2019;29(6):2890–901.
38. Peng YT, Zhou CY, Lin P, et al. Preoperative Ultrasound Radiomics Signatures for Noninvasive Evaluation of Biological Characteristics of Intrahepatic Cholangiocarcinoma. Acad Radiol. 2020;27(6):785–97.
39. Mao Y, Jiang L, Wang JL, et al. Radiomic nomogram for discriminating parotid pleomorphic adenoma from parotid adenolymphoma based on grayscale ultrasonography. Front Oncol. 2023;13:1268789.
40. Xiao ML, Fu L, Wei Y, et al. Intratumoral and peritumoral MRI radiomics nomogram for predicting parametrial invasion in patients with early-stage cervical adenocarcinoma and adenosquamous carcinoma. Eur Radiol. 2024;34(2):852–62.
41. Tang VH, Duong STM, Nguyen CDT, et al. Wavelet radiomics features from multiphase CT images for screening hepatocellular carcinoma: analysis and comparison. Sci Rep. 2023;13(1):19559.
42. He W, Tang M, Jiang X, et al. Visual interpretation of Radiomics Features in filtered computed tomography images during the Portal Phase of Acute Pancreatitis. Discov Med. 2024;36(183):730–8.
43. Granata V, Fusco R, De Muzio F, et al. Radiomics textural features by MR imaging to assess clinical outcomes following liver resection in colorectal liver metastases. Radiol Med. 2022;127(5):461–70.
44. Bicci E, Calamandrei L, Di Finizio A, et al. Predicting Response to Exclusive Combined Radio-Chemotherapy in Naso-Oropharyngeal Cancer: the role of texture analysis. Diagnostics (Basel). 2024;14(10):1036.

Publisher's note

Springer Nature remains neutral with regard to jurisdictional claims in published maps and institutional affiliations.